New Conceptual Framework for the Erosion of Fine Sediment from a Gravel Matrix Based on Experimental Analysis

Giulia Stradiotti[1], Maurizio Righetti[2], Tesfaye Haimanot Tarekegn[3], Geraldene Wharton[4], and Marco Toffolon[5]

[1]Faculty of Science and Technology, Free University of Bozen-Bolzano, Piazza Università 1, 39100 Bozen-Bolzano, Italy. Email: gstradiotti@unibz.it

[2]Faculty of Science and Technology, Free University of Bozen-Bolzano, Piazza Università, 1, 39100 Bozen-Bolzano, Italy. Email: maurizio.righetti@unibz.it

[3]School of Geography and Earth Sciences, McMaster University, 1280 Main Street West Hamilton, Ontario, Canada, Department of Civil, Environmental and Mechanical Engineering, University of Trento, Via Mesiano 77, 38123 Trento, Italy and School of Geography, Queen Mary University of London, Mile End Road, London E1 4NS, United Kingdom. Email: tarekegt@mcmaster.ca

[4]School of Geography, Queen Mary University of London, Mile End Road, London E1 4NS, United Kingdom. Email: g.wharton@qmul.ac.uk

[5]Department of Civil, Environmental and Mechanical Engineering, University of Trento, Via Mesiano 77, 38123 Trento, Italy. Email: marco.toffolon@unitn.it

ABSTRACT

An experimental non-intrusive methodology is proposed to estimate the spatially averaged erosion rate of fine sediment from a gravel bed. The experiments performed in a laboratory flume show a progressive slow-down of the erosion rate as the level of fine sediment becomes deeper within the gravel matrix, until a maximum depth of erosion is reached. Two original relations are proposed for the maximum cleanout depth and the erosion rate, based on a dimensional analysis applied to the experimental results. The proposed erosion rate relation modifies the original Van Rijn formula for uniform bed, introducing a damping function below the gravel crest. Both the evolution of the erosion rate with depth and the maximum depth of erosion can be defined as simple functions of the general characteristics of the flow and the fine and coarse fractions of the sediment. Our approach will lead to improved estimates of the conditions under which fine sediments that have infilled gravel beds are re-entrained. This will help inform strategies aimed at restoring degraded river systems and mitigating the undesired side effects of activities such as sediment flushing which can result in colmation.

Keywords: Sediment erosion; Sediment entrainment; Sediment transport; Gravel bed river; Clogging; Winnowing

INTRODUCTION

Streambed colmation or clogging, in which excess fine sediment is deposited within the coarser matrix of river beds, altering their structure, reducing porosity, and hydraulic conductivity, is a global problem (Wharton et al., 2017). It has been linked to past and on-going human activities including deforestation, agricultural practices, mining activities, urbanization, and river engineering (Wood and Armitage 1997). River impoundments reduce downstream flows of water and fine sediment transport (Petts 1984) and can lead to river bed armoring as a consequence of fine sediment winnowing. But sediment flushing operations to mitigate progressive reservoir siltation and dam removal at the end of a reservoir's lifespan trigger the sudden release of large volumes of fine sediment and are a cause of colmation and a wide range of associated environment impacts (Gray and Ward 1982; Wohl and Cenderelli 2000; Crosa et al. 2010; Asaeda and Rashid 2012; Hug Peter et al. 2014).

Declogging of riverbeds can be undertaken by mechanical removal ("vacuuming") of fine sediments, but this is only realistic in smaller rivers and streams in targeted areas. Releasing clean "flushing" flows from upstream reservoirs is a more widespread remediation technique (Wu and Chou 2004), and it can help to restore river ecosystems, but further research is needed to guide environmentally sensitive flushing as part of mitigation and restoration strategies (Kondolf et al. 2014). This requires more detailed understanding of the interaction between flows, fine sediment, and coarse quasi-immobile gravel beds and the resultant transport dynamics. Indeed, the effectiveness of the decolmation is directly related to the maximum depth from which sediment can be entrained given a certain flow, and to the erosion rate of fine sediments from the gravel matrix, which affects the suspended transport capacity. From a modelling perspective, the concentration profile and the corresponding suspended sediment transport rate are intrinsically dependent on the boundary condition set at the bed. This boundary condition has been widely defined in the literature for river beds covered by uniform material, where it is expressed through different parameterizations of the erosion rate at the bed (e.g., Van Rijn 1984; Garcia and Parker 1991; Engelund and Fredsoe 1976).

However, little is known about the erosion of non-uniform beds, where fine sediment is suspended and transported over a coarse immobile gravel bed. In such conditions, that are typical of riverbeds downstream of dams (Kondolf 1997), the flow over the coarse boundary can be properly specified by accounting for the three-dimensional spatial heterogeneity of the bed in the governing equations. This is achieved through the double-averaging approach (Nikora et al. 2001), which introduces two new types of terms in the momentum equation: drag terms and form-induced momentum fluxes. Recent studies investigated the structure of turbulence following the double-averaging approach in rough beds with clear water, where detailed measurements of velocities are possible (e.g., Mignot et al. 2009; Dey and Das 2012; Mohajeri et al. 2015; Mohajeri et al. 2016), and found out that sweeps events prevail far below the gravel crest, whereas form-induced fluxes are relevant only in a narrow region around it. These modifications to the turbulence structure caused by the protrusion of the gravel, which at the same time acts as a drag to the flow adsorbing part of the flow momentum (Nikora et al. 2001), are expected to reduce the sediment entrainment capacity of the flow. Another decreasing factor is the reduced active surface: below the gravel crest, the fine sediment-water interface is just the portion of the bed corresponding to the horizontal porosity among the coarse grains, also defined as roughness geometric function (Nikora et al. 2001). These findings on the turbulence behavior and on the structure of the bed suggest that the erosion rate should decrease with the fine sediment level, reducing the sediment transport rate compared to that from a uniform bed, as confirmed by experimental results (e.g. Grams and Wilcock 2007; Grams and Wilcock 2014; Kuhnle et al. 2013; Kuhnle et al. 2017).

Past studies measured the concentration of suspended particles as a proxy for the fine sediment entrainment rate, or exploited stop and run procedures to evaluate the influence of the fine sediment level within the gravel matrix on the fine sediment transport rate (e.g., Kuhnle et al. 2013; Kuhnle et al. 2016; Kuhnle et al. 2017). However, due to the structure of a gravel bed, direct and continuous measurements of the interaction between fine sediment and gravel are still missing.

Following recent developments in using optical techniques to measure river bed evolution (e.g. Huang et al. 2010; Soares-Frazão et al. 2007; Limare et al. 2011), in this study we adopted a non-intrusive laser line / video camera technique that allowed for direct and continuous measurements of fine sediment bed evolution (section 2) which avoided the need to analyse the turbulent flow below the gravel crest and its damping effect. Based on the experimental data, we defined an empirical formulation for the erosion rate (section 4), in the form of an updated Van Rijn (1984) formula. As the formula was originally derived through laboratory experiments using a uniform bed, it does not account for the presence of the macro-roughness, and the consequent reduction of the erosion rate below the gravel crest level.

MATERIALS AND METHODS

New Experimental Data

Experiments were carried out in a laboratory flume in the Department of Civil, Environmental and Mechanical Engineering (DICAM) of the University of Trento, under varying conditions of discharge, slope and fine sediment size (figure 1). The flume was 16 m long, 0.4 m wide and 0.7 m deep, with a plastic left wall and a glass right wall, both smooth (for further details on the experimental set-up see Tarekegn (2015)). The water was fed in the flume from a 15 m^3 tank by a recirculating pump passing through a gate valve, and measured by an electromagnetic flow meter connected to the inlet pipe, with a maximum error of 0.005 Q, where Q is the water discharge.

Water level for a given discharge downstream was controlled by a manual floodgate to maintain uniform flow conditions.

The bed of the flume was filled to a depth of 20 cm with gravel (D_{90} = 30.44 mm), leveled out with a wooden plate, and water worked. Before the addition of fine sediment, the gravel bed surface was characterized using a M5L/200 laser scanner (MEL Mikroelektronik, vertical resolution 0.1 mm) to obtain the gravel crest height, set as Z_{99} of the CPDG (cumulative probability distribution of gravel), i.e. the level for which 99% of the gravel elevations are lower.

The measurement section was 12.2 cm long and 20 cm wide, and positioned 7.8 m from the flume entrance, where fully developed boundary flow was reached (Kirkgöz and Ardiçlioğlu 1997). In the measurement section, the gravel was filled with bakelite (specific gravity = 1.553), whereas in the rest of the flume the gravel was filled with sand (d_{50} = 1.25 mm, specific gravity 2.670) up to the crest level. The sand was used to shield the measurement section, avoiding the possibility that erosion would be affected by discontinuities in sediment infilling upstream and downstream the measurement section. At the imposed flow conditions, the chosen sand size is not entrained, thus it does not affect the sediment transport. To prevent erosion below the gravel crest before the establishment of uniform flow conditions, the bakelite sediment were filled above the crest level in the flume up to two thirds of the flow depth. Bakelite was chosen because its low density makes it particularly suitable to be transported in suspension. It had uniform diameter $d_s = 425\ \mu$m in 7 runs, and $d_s = 500\ \mu$m in 2 runs. Bakelite porosity was $p = 0.46$. Please note that the gravel grain size is denoted with the capital letter, D, and the bakelite grain size with the lower letter, d.

The established flow was a type 1 (Nikora et al. 2001), subcritical flow (Froude number $Fr < 1$) mainly characterized by suspended transport for bakelite sediment (Rouse number $Ro < 1$ for bakelite sediment and $Ro > 1$ for sand; flow characteristics are summarized in Table 1). We calculated shear velocity at the gravel crest level (subscript 0) u_{*0} as:

$$u_{*0} = \sqrt{\frac{\tau_0}{\rho}}, \tag{1}$$

with ρ water density and the bed shear stress τ_0 defined as:

$$\tau_0 = g \, \rho \, S_0 \, R_b \, , \tag{2}$$

where R_b is the hydraulic radius with the sidewall correction by Cheng (2011) to account for the different hydraulic resistance between bed and sidewalls.

The experiments aimed to evaluate the erosion of bakelite sediment by following the progressive lowering of a green laser line projected on the sediment bed. Each video footage was captured with a Sony DCR-VX200 DV (768 pixel × 576 pixel resolution, 25 frames per second) filming a mirror reflecting the flume bottom, where the laser was projected (figure 2). The laser was a FLEXPOINT FP-53/4F-O30-HOM (wavelength 532 nm, output power 10 mW, fan angle 30°), projecting a green light. Since the experiments were filmed in running water, a Plexiglas lamina was lent on the water surface to reduce signal distortion caused by refraction at air-water boundary and surface turbulence (figure 2). The videos were recorded on Mini DV cassettes, keeping the light off and the video camera shutter narrow to enhance the contrast between the green laser light and the background. The video records were then extracted in uncompressed format using Windows Movie Maker®. From each video we analyzed images every 60 frames (2.4 s) in bitmap format, which records colors in RGB code. Using MATLAB®, we converted the images in grayscale, obtaining for each image a matrix containing the position of the laser line. Using a mirror allowed for a better resolution in the vertical scale, which would not have been possible with the camera recording perpendicularly the bottom of the flume. We made the conversion from pixel to mm through calibration images, extracted from videos in which a calibration rod 104 mm long was moved for a step of 10 mm in the vertical plane. Knowing the length of the rod and counting the pixels horizontally occupied by it, we were able to obtain the horizontal conversion scale. As for the vertical scale, the conversion was made by counting the difference in pixels from position 1 to position 2 in the vertical plane, equal to the known movement of 10 mm (see figure 3). We repeated the procedure for each of the 9 runs. The mean values for the conversion scales (which present small differences among the 9 runs) are $H_h = 0.174$ mm/pixel and $H_v = 0.381$ mm/pixel for the vertical scale. Given that bakelite sediments had diameter $d_s = 0.425$ mm or $d_s = 0.500$ mm, the resolution coming from the conversion scale allowed for a bakelite particle to be described by more than one pixel.

The erosion rate can be computed locally as

$$E(z) = -(1-p)\frac{\partial z}{\partial t}, \tag{3}$$

where p is the bakelite sediment porosity. When the bakelite level z is known along the laser line at a certain instant t, the spatially-averaged erosion rate $\langle E\rangle(\langle z\rangle)$ can be easily obtained (the angle brackets representing spatial averaging will be dropped in the remaining part) (figure 4). The substitution of the spatial average by the average computed on a line is possible for fully developed flows choosing an adequate length of the line $L_x \sim 5-6\,D_{50}$, that is about 10 times the saturation length of the bed elevation variogram ($\sim 0.5\ D_{50}$, Mohajeri et al. 2015), where D_{50} is the median value of the CPDG. Details on the pre-processing of the images, on the extraction of the laser centerline and on the spatial average computation are provided in Appendix I.

For the analysis of the erosion of fine sediment, we set the reference system origin at the gravel crest level, $z_c = 0$, with time $t = 0$ when the bakelite reached that level. The gravel crest was identified at the level Z_{99} of the CPDG. The whole analysis was focused on the interfacial sub-layer (Nikora et al. 2001), that is the layer in which the gravel exerts the greatest influence. In our reference system, the top of the interfacial sub-layer is set at the level $z = 0$.

Other Datasets

In our experiments, we performed measurements over a small range of u_* ($0.023 \div 0.031\ m/s$). To overcome this limit, we compared the maximum depths of erosion z_{max} measured in our experiments with the ones measured by Kuhnle et al. (2016). For their experiments, Kuhnle et al. (2016) applied a variety of flow-rates with u_* ranging up to 0.9 times the critical u_* for gravel. They carried out experiments in a laboratory flume using 3 sets of sands, with diameter 0.2 mm, 0.3 mm and 0.86 mm, respectively, obtaining 20 cleanout depth data. Whereas in this study we directly measured the lowering of bakelite over time, defining the maximum depth of erosion as the final depth achieved that did not change over time, Kuhnle et al. (2016) defined it as a function of sand concentration (where sand represented the fine fraction, as bakelite in our experiments) and they measured the sand level established in the flume when the concentration of the sand in the flow exiting the flume was less than or equal to 0.5 mg/L.

Empirical Relations from Previous Studies

In this study, we defined the erosion rate by updating the empirical formulation provided by Van Rijn (1984) in non-equilibrium transport. Van Rijn (1984) used a step-and-go procedure, measuring erosion as the mass ΔM of sediment removed from an area A per unit time Δt, under uniform flow conditions:

$$e_{VR} = \frac{\Delta M}{A\,\Delta t}\,. \tag{4}$$

Van Rijn (1984) related the mass erosion rate e_{VR} to the dimensionless particle parameter d_* and the dimensionless transport-stage parameter T (Van Rijn 1981; Van Rijn 1982):

$$e_{VR} = \varepsilon\, {d_*}^{0.3}\, T^{1.5} \rho_s \sqrt{R\, g\, d_{50}}\,. \tag{5}$$

In equation (5), the dimensionless grain size d^* is defined as

$$d_* = d_{50} \left(\frac{R\,g}{\nu^2}\right)^{1/3}\,, \tag{6}$$

where d_{50} is the median sediment diameter of the particle distribution, $R = (\rho_s - \rho)/\rho$ is the relative density, with ρ_s the sediment density and ρ the water density, g is the acceleration of gravity, and ν is the kinematic viscosity. The dimensionless excess shear stress T is defined as:

$$T = \frac{u_*^2 - u_{*cr}^2}{u_{*cr}^2}\,, \tag{7}$$

where $u_{*,cr}$ is the critical shear velocity according to Shields criterion. Finally, the proportionality coefficient calibrated by Van Rijn (1984) was $\varepsilon = 0.00033$.

Hereafter, we adopt $E_0 = e_{VR}/\rho_s$ as the reference volumetric erosion rate.

THEORETICAL DEVELOPMENT

One of the key features in fine sediment entrainment from a gravel bed is the maximum depth of erosion z_{max} associated with given hydraulic conditions. This parameter represents the lower limit of the erosive process and determines the temporal scale of the phenomenon. A dimensional analysis allowed us to express the maximum depth of erosion z_{max} as a function of flow and sediment characteristics. We assumed that z_{max} depends on the geometric characteristics of both fine and coarse sediment, on the density of fine sediment ρ_s, and on the characteristics of the flow on the gravel crest:

$$z_{max} = f(D_{90}, d_s, \rho, \rho_s, \tau_0, g, \mu)\,, \tag{8}$$

where d_s is the characteristic grain size of fine sediment (in this study equal to d_{50}) and τ_0 refers to the shear stress at gravel crest level, whereas μ is the dynamic viscosity. Using ρ, g, d_s as internal scales, equation (8) becomes

$$\frac{z_{max}}{d_s} = F\left(\frac{D_{90}}{d_s}, \frac{\rho_s}{\rho}, \frac{u_{*0}^2}{g\,d_s}, \frac{\mu}{\rho\sqrt{g}\,d_s^{3/2}}\right). \tag{9}$$

If properly combined with the relative density $R(= \rho_s/\rho - 1)$, the third non-dimensional group can equate to the Shields parameter for fine sediment referred to the gravel crest level:

$$\theta_0 = \frac{u_{*0}^2}{g\,d_s} \cdot \frac{1}{R}\,. \tag{10}$$

The fourth parameter can be written as the reciprocal of the dimensionless grain size:

$$d_*^{-1} = \left(\frac{\mu}{\rho\sqrt{g}\,d_s^{3/2}}\right)^{-2/3} \cdot R^{-1/3}, \tag{11}$$

where the expression in brackets identifies the reciprocal of the Reynolds particle number. This parameter can be ultimately used to obtain the critical Shields parameter for incipient motion (Brownlie 1981):

$$\theta_{cr} = 0.22\, d_*^{-0.9} + 0.06 \cdot 10^{-7.7\, d_*^{-0.9}} \,. \tag{12}$$

Finally, making the hypothesis that z_{max} does not depend on θ_0, but on the excess of θ_0 compared to θ_{cr}, following Van Rijn (1984) we defined the dimensionless excess of shear stress at the gravel crest as

$$T_0 = \frac{u_{*0}^2 - u_{*cr}^2}{u_{*cr}^2} = \frac{\theta_0 - \theta_{cr}}{\theta_{cr}} \,, \tag{13}$$

that expresses the surplus of energy of the flow with comparison to the amount needed to overcome the threshold of incipient motion of the fine sediment. This allowed us to reduce the number of parameters in equation (9) and simplify it as

$$\frac{z_{max}}{d_s} = \widehat{F}\left(\frac{D_{90}}{d_s}, T_0\right) = \frac{D_{90}}{d_s} \cdot \widehat{G}\left(\frac{D_{90}}{d_s}, T_0\right) . \tag{14}$$

Further assuming that for $D_{90}/d_s \to \infty$ (i.e., gravel much larger than fine sediment) the dependence on this ratio can be neglected in $\widehat{G}$, and relation (14) can be written in dimensionless form:

$$\frac{z_{max}}{D_{90}} = \widehat{f}(T_0) \,. \tag{15}$$

RESULTS

Maximum Depth of Erosion

Equation (15) that we presented in section 3 was tested using two sets of data: the set of z_{max} resulting from this study, and one from the literature (Kuhnle et al. 2016) (see section 2). We note that the analysis is meaningful only in a range of u_{*0} for which the coarse material does not move. We assumed a simple power-law formulation for equation (15) as:

$$\frac{z_{max}}{D_{90}} = -a\, T_0^b \,, \tag{16}$$

where the minus sign accounts for the fact that the cleanout depth is negative by definition. The calibration of the coefficients of this formula with the available data sets provided $a = 0.32$ and $b = 0.37$ (figure 5), evaluated by least squares interpolation.

Erosion Rate Below the Gravel Crest

The erosion rate of fine sediment at the gravel crest, E_0, was defined assuming that the gravel does not have any effect on the erosion dynamics until the crests are uncovered. When the gravel crest is fully covered by fine sediment and it is not exposed to the flow, then E_0 can be expressed using a uniform-bed formula. As introduced in section 2, in this study we used the well-known Van Rijn (1984) relation (hereafter, VR) for the volumetric erosion flux:

$$E_0 = \frac{e_{VR}}{\rho_s} = \varepsilon T_0^{1.5} d_*^{0.3} \sqrt{gRd_{50}}\,, \tag{17}$$

Below the gravel crest level, the momentum flux is affected both by form-induced stress and form drag terms (Nikora et al. 2001), hence VR is not directly applicable because the total shear stress used in the evaluation of T_0 does not account for this different allocation of the contributions (i.e. form drag, Reynolds stresses, form-induced stresses).

Our experimental results show that the erosion rate reduces progressively below the gravel crest (figure 6), in accordance with findings previously reported in the literature: form-induced stresses contribute to the total erosion rate in the region around the gravel crest, whereas going further in depth net vertical fluxes are mostly directed downwards (Mohajeri et al. 2016). This decline in the erosion rate varies among the runs, responding to the changes in slope, discharge and water depth, which can be all summarized in the change of the shear velocity u_{*0}. The runs with higher shear velocity have a fast lowering of z in the beginning of the process, and erode to a deeper level. Given these premises, we defined the decline in the erosion rate as a modification of the reference erosion rate predicted by VR:

$$E(z) = E_0\left[1 - \left(\frac{z}{z_{max}}\right)^m\right], \qquad (z > z_{max})\ . \tag{18}$$

The structure of equation (18) implies that, below the gravel crest level, the erosion rate decreases with a power law of the depth, and vanishes at $z(t) = z_{max}$. The maximum depth of erosion, z_{max}, can be estimated from (16), and the coefficient $m = 0.202$ was set as the mean value among the exponents resulting from the fitting on each experimental run. A summary of $E(z)$ for all runs is plotted in figure 7. The erosion rate $E(z)$ in non-equilibrium transport is related to $z(t)$ by means of equation (3), which can be numerically integrated to obtain $z(t)$:

$$z(t + \Delta t) = z(t) - \frac{E(z)}{1 - p}\Delta t \,. \tag{19}$$

Note that the origin for z is set at the gravel crest level, so that at greater depths the ratio z/z_{max} gets larger. Even if relation (18) in its formulation does not present a proper mathematical asymptote, and it is defined until it reaches $E = 0$, figures (6) and (7) show a quasi-asymptotic trend when z approaches z_{max}.

DISCUSSION

Our measurements show a decrease in the erosion rate of fine sediment below the gravel crest, from which we defined a new relation for the erosion rate $E(z)$. We assumed that a uniform-bed formula is valid as long as the gravel matrix is still covered by fine sediment, that is, until the gravel crest level is reached, but thereafter it has to be updated for decreasing z. Hence, we defined $E(z)$ as a fraction of the reference value E_0, computed using Van Rijn (1984) (eq. 18). Such a relation presents a rapid decrease in the erosion rate in the early stages (close to the gravel crest) with an adjustment to lower erosion rates until z_{max} is reached (figures 6, 7). The maximum depth of erosion z_{max} used in equation (18) was derived through a dimensional analysis (eq. 15), that relates the maximum erosion depth with the dimension of the gravel and the excess of shear stress at the gravel crest (figure 5). The dimension of the gravel is represented in equation (15) by D_{90}, whereas the excess of shear stress at the gravel crest level is represented by the non-dimensional parameter T_0, that gives the relation between the limits of the erosive process and the energy of the mean flow. Both z_{max} and $E(z)$ are written as functions of u_{*0}, that subsumes the varying parameters among the different runs (H, Q, S). Higher shear velocities are mirrored in higher non-dimensional excesses of shear stress, which produce erosive processes that run out at deeper levels (eq. 15), but have an influence also in the initial phases, where higher shear velocities force higher E_0 and consequently faster lowering of z level (eq. 18). We acknowledge that our experiments were carried out over a limited range of u_*, but the inclusion of a wider data set (Kuhnle et al. 2016) into the analysis to derive equation (16) ensures the results have a wider significance. Importantly, since the values of u_* in the dataset by Kuhnle et al. (2016) ranged up to 0.9 times the critical shear velocity for gravel entrainment, equation (16) suggests a limit to the erosive process, whereby it is not possible to entrain fine sediment below a distance of $\sim 2\ D_{90}$ from the crest without also moving the gravel.

Other sources of uncertainty are related to the calibration of the parameters. We obtained the curve of $E(z)$ and its numerical integral $z(t)$ from the experimental data imposing the averaged value of the exponent m. In the time period immediately after the uncovering of the gravel crest, some oscillations in the erosion rate (figures 6 and 7) were measured, due to the change in the macro-roughness of the bed and the increase in turbulence. These oscillations are not represented by the model, which expresses the evolution of the erosion rate just as a function of z, and this explains the discrepancy in some points between the analytical representation of $z(t)$ and the experimental data (figures 6 and 7). An additional source of uncertainty is introduced by imposing that the erosive process ends when the level reaches z_{max}, a parameter that would need more experimental observations to be definitively estimated. These uncertainties are justified in the framework of a simplified model that only requires the mean flow characteristics to describe the continuous evolution of the erosion of fine sediment below the gravel crest. It is important to note that the properties of the gravel matrix affect large scale processes. The erosion rate of the fine sediment is experimentally measured in the voids of the gravel bed, that is, the portion of the bed in which the fine sediments are in direct contact with the water (see Appendix I). Hence, at a chosen z level, the total erosion rate E_g considering the whole bed surface depends on the porosity of the gravel $\phi(z)$, providing the following expression:

$$E_g(z) = E(z) \cdot \phi(z)\ . \tag{20}$$

Therefore, the Exner equation for fine sediment transport in gravel bed rivers,

$$\frac{\partial q_s}{\partial x} + \rho_s(1-p)\frac{\partial z}{\partial t}\phi(z) = 0\,, \tag{21}$$

where q_s is the mass transport rate per unit width, can be recast as:

$$\frac{\partial q_s}{\partial x} = \rho_s E_g(z)\,. \tag{22}$$

Since $E_g(z) < E_0$, both because of the different distribution of the stresses and because of the reduction of the fine sediment-water interface with comparison to a uniform bed, the reduced entrainment capacity causes a parallel reduction in the transport capacity, as previous studies confirm (e.g., Kuhnle et al. 2013).

The new conceptual framework we propose has the potential to be easily applicable to real-world situations. This is because equation (18) includes two variables that can be estimated on the basis of the characteristics of the flow at the gravel crest level, and that only requires simple parameters (size, density) of fine sediment and gravel to be specified. In fact, z_{max} is obtained from equation (16) and E_0 from VR.

The proposed erosion rate formula can also be used to set the boundary condition at the bottom, $<\bar{c_a}>$, for the computation of the suspended sediment profile in equilibrium conditions. The standard procedure for a uniform sand bed is illustrated, for instance, by Garcia and Parker (1991), whereas in the case of fine sediment transport over a gravel bed, the double-averaging approach must be applied to the advection-diffusion equation (Nikora et al. 2007; Nikora et al. 2013). At a reference depth a sufficiently close to the fine sediment bed, the equilibrium concentration $<\overline{c_{ae}}>$ can be written as:

$$<\overline{c_{ae}}> = \frac{E_a}{\omega_s}\,, \tag{23}$$

with $E_a = E(z = a)$. Since the erosion rate continues to decline with increasing depth in the gravel matrix, the contribution E_a needs to be adjusted in accordance with the function $E(z)$ that we proposed in equation (18). Hence, the equilibrium concentration decreases as well, which in turn affects the suspended sediment load. Therefore, our findings have important implications for the computation of fine sediment transport over a coarse gravel bed.

CONCLUSIONS

Streambed colmation is a major cause of the ecological degradation of rivers on a global scale and more detailed understanding of the mechanisms of both colmation and decolmation is required to help develop environmentally sensitive management operations. Improved insight is needed to mitigate the worst impacts of sediment releases from hydropower schemes and guide the use of clean flushing flows (Wharton et al. 2017; Wilkes et al. 2019). In particular, the use of flushing flows to remove fine sediments deposited within coarse stream beds needs to be informed by improved knowledge of how spatial variations in streambed morphology and hydraulic conditions create areas with different levels of susceptibility to decolmation. Our study provides valuable insights into what happens to erosion rates in the zones below the gravel crest where fine sediments are trapped within the gravel matrix and our approach will contribute to improving predictions of the erosion rates required for decolmation.

Predicting the erosion rate of fine sediment from a gravel bed is problematic due to the temporal and spatial variability of the stresses at the bed. We performed and recorded experiments in a laboratory flume adopting a non-intrusive technique, which combined a mirror, a laser and a video camera. The laser line projected on the sediment bed mirrors the lowering of the fine sediment level within the coarse gravel matrix over time. Using this methodology, we obtained direct and continuous measurements of the phenomenon, which enabled us to formulate an empirical relation for the erosion rate below the gravel crest (equation 18), which decreases with comparison to the case of a uniform bed (figure 6).

The erosion rate, $E(z)$, progressively decreased below the gravel crest until it ceased at the maximum depth of erosion, z_{max}. Such a depth was found to scale well with the excess shear stress, T_0, at the gravel crest level, whereas $E(z)$ was estimated as a decreasing function of z. Unfortunately, to our best knowledge, no other similar experimental datasets are available, hence further experiments should be carried out to validate the proposed model for $E(Z)$ and $z(t)$.

Both $E(Z)$ and $z(t)$ were expressed in terms of the general characteristics of the flow at the gravel crest and of the characteristics of the fine and coarse materials. These parameters are usually known or can be easily obtained, which makes the estimation of the erosion rate using this approach easier compared to formulae that require computation of the cumulative distribution of gravel. Moreover, the estimation of the erosion rate near the fine sediment level can also be used to set the boundary condition for the concentration profile and, hence, to compute the suspended sediment transport over a coarse bed.

DATA AVAILABILITY STATEMENT

Some of the data, models, or code generated or used during the study are available from the corresponding author by request:

- text files of bakelite depth vs. time $z(t)$ for each run;
- Excel file with the characteristics of each run.

ACKNOWLEDGEMENTS

The authors would like to thank the anonymous reviewers, whose valuable suggestions helped improve the quality of this manuscript. Part of the research was carried out during the doctoral research of T.H. Tarekegn, supported by the Erasmus Mundus Doctorate Program SMART (http://www.riverscience.eu) funded by the Education, Audiovisual and Culture Executive Agency (EACEA) of the European Commission, and part has been supported by the CDC project "HM, Sustainable management of hydroelectric production, Hydropeaking Mitigation: morphological mitigation measures assessment", funded by the Free University of Bozen-Bolzano.

REFERENCES, CITATIONS AND BIBLIOGRAPHIC ENTRIES

REFERENCES

Asaeda, T. and Rashid, M. H. (2012). “The impacts of sediment released from dams on downstream sediment bar vegetation.” *Journal of Hydrology*, 25–38.

Brownlie, W. R. (1981). “Prediction of flow depth and sediment discharge in open channels.” *Report No.KH-R-43A*, W.M. Keck Laboratory of Hydraulics and Water Resources, Division of Engineering and Applied Science, California Institute of Technology, Pasadena, California.

Cheng, N.-S. (2011). “Revisited vanoni-brooks sidewall correction.” *International Journal of Sediment Research*, 26, 524–528.

Crosa, G., Castelli, E., Gentili, G., and Espa, P. (2010). “Effects of suspended sediments from reservoir flushing on fish and macroinvertebrates in an alpine stream.” *Aquatic Sciences*, 72, 85–95.

Dey, S. and Das, R. (2012). “Gravel-bed hydrodynamics: Double-averaging approach.” *Journal of Hydraulic Engineering*, 138, 707–725.

Engelund, F. and Fredsoe, J. (1976). “A sediment transport model for straight alluvial channel.” *Nordic Hydrology*, 7, 293–306.

Garcia, M. and Parker, G. (1991). “Entrainment of bed sediment into suspension.” *Journal of Hydraulic Engineering*, 117, 414–435.

Gonzalez, R., Woods, R., and Eddins, S. (2004). *Digital Image Processing Using MATLAB*. Pearson Prentice Hall.

Grams, P. E. and Wilcock, P. R. (2007). “Equilibrium entrainment of fine sediment over a coarse immobile bed.” *Water Resources Research*, 43.

Grams, P. E. and Wilcock, P. R. (2014). “Transport of fine sediment over a coarse, immobile riverbed.” *Journal of Geophysical Research: Earth Surface*, 119(2), 188–211.

Gray, L. J. and Ward, J. V. (1982). “Effects of sediment releases from a reservoir on stream macroinvertebrates.” *Hydrobiologia*, 96, 177–184.

Huang, M. Y., Huang, A. Y., and Capart, H. (2010). “Joint mapping of bed elevation and flow depth in microscale morphodynamics experiments.” *Experiments in fluids*, 49(5), 1121–1134.

Hug Peter, D., Castella, E., and Slaveykova, V. (2014). “Effects of a reservoir flushing on trace metal partitioning, speciation and benthic invertebrates in the floodplain.” *Environ. Sci.: Processes Impacts*.

Kirkgöz, M. S. and Ardiçlioğlu, M. (1997). "Velocity profiles of developing and developed open channel flow." *Journal of Hydraulic Engineering*, 123(12), 1099–1105.

Kondolf, G. M. (1997). "Hungry water: Effects of dams and gravel mining on river channels." *Environmental Management*, 21(4), 533–551.

Kondolf, G. M., Gao, Y., Annandale, G. W., Morris, G. L., Jiang, E., Zhang, J., Cao, Y., Carling, P., Fu, K., Guo, Q., Hotchkiss, R., Peteuil, C., Sumi, T., Wang, H.-W., Wang, Z., Wei, Z., Wu, B., Wu, C., and Yang, C. T. (2014). "Sustainable sediment management in reservoirs and regulated rivers: Experiences from five continents." *Earth's Future*, 2(5), 256–280.

Kuhnle, R. A., Langendoen, E. J., and Wren, D. G. (2017). "Prediction of sand transport over immobile gravel from supply-limited to capacity conditions." *Journal of Hydraulic Engineering*, 143.

Kuhnle, R. A., Wren, D. G., and Langendoen, E. J. (2016). "Erosion of sand from a gravel bed." *Journal of Hydraulic Engineering*, 142.

Kuhnle, R. A., Wren, D. G., Langendoen, E. J., and Rigby, J. R. (2013). "Sand transport over an immobile gravel bed substrate." *Journal of Hydraulic Engineering*, 139, 167–176.

Limare, A., Tal, M., Reitz, M. D., Lajeunesse, E., and Métivier, F. (2011). "Optical method for measuring bed topography and flow depth in an experimental flume." *Solid Earth*, 2(2), 143–154.

Mignot, E., Barthelemy, E., and Hurter, D. (2009). "Double-averaging analysis and local flow chracterization of near-bed turbulence in gravel-bed channel flow." *Journal of Fluid Mechanics*, 618, 279–303.

Mohajeri, S. H., Grizzi, S., Righetti, M., Romano, G. P., and Nikora, V. (2015). "The structure of gravel-bed flow with intermediate submergence: A laboratory study." *Water Resources Research*, 51, 9232–9255.

Mohajeri, S. H., Righetti, M., Wharton, G., and Romano, G. P. (2016). "On the structure of gravel-bed flow with intermediate submergence: implications for sediment transport." *Advances in Water Resources*, 92, 90–104.

Nikora, V., Ballio, F., Coleman, S., and Pokrajac, D. (2013). "Spatially averaged flows over mobile rough beds: definitions, averaging theorems, and conservations equations." *Journal of Hydraulic Engineering*, 139, 803–811.

Nikora, V., Goring, D., McEwan, I., and Griffiths, G. (2001). "Spatially averaged open-channel flow over rough bed." *Journal of Hydraulic Engineering*, 127, 123–133.

Nikora, V., McEwan, I., McLean, S., Coleman, S., Pokrajac, D., and Walters, R. (2007). "Double-averaging concept for rough-bed open-channel and overland flows: theoretical background." *Journal of Hydraulic Engineering*, 133, 873–883.

Petts, G. E. (1984). "Sedimentation within a regulated river." *Earth Surface Processes and Landforms*, 9(2), 125–134.

Soares-Frazão, S., Grelle, N. L., Spinewine, B., and Zech, Y. (2007). "Dam-break induced morphological changes in a channel with uniform sediments: measurements by a laser-sheet imaging technique." *Journal of Hydraulic Research*, 45(sup1), 87–95.

Sung, K., Lee, H., Choi, Y. S., and Rhee, S. (2009). "Development of a multiline laser vision sensor for joint tracking in welding." *Supplement to the Welding Journal*, 88, 79–85.

Tarekegn, T. H. (2015). "Downstream suspended sediment dynamics of reservoir sediment flushing." Ph.D. thesis, University of Trento, Trento, Italy.

Van Rijn, L. C. (1981). "Computation of bed-load concentration and bed-load transport." *Report No. S 487-I*, Delf Hydraulics Laboratory, Delft, Netherlands.

Van Rijn, L. C. (1982). "Computation of bed-load concentration and suspended-load transport." *Report No. S 487-II*, Delf Hydraulics Laboratory, Delft, Netherlands.

Van Rijn, L. C. (1984). "Sediment pick-up functions." *Journal of Hydraulic Engineering*, 110, 1494–1502.

Wharton, G., Mohajeri, S. H., and Righetti, M. (2017). "The pernicious problem of streambed colmation: a multi-disciplinary reflection on the mechanisms, causes, impacts, and management challenges." *Wiley Interdisciplinary Reviews: Water*, 4.

Wilkes, M. A., Gittins, J. R., Mathers, K. L., Mason, R., Casas-Mulet, R., Vanzo, D., Mckenzie, M., Murray-Bligh, J., England, J., Gurnell, A., and Jones, J. I. (2019). "Physical and biological controls on fine sediment transport and storage in rivers." *WIREs Water*, 6(2), e1331.

Wohl, E. and Cenderelli, D. A. (2000). "Sediment deposition and transport patterns following a reservoir sediment release." *Water Resources Research*, 36, 319–333.

Wood, P. J. and Armitage, P. D. (1997). "Biological effects of fine sediment in the lotic environment." *Environmental Management*, 21(2), 203–217.

Wu, F.-C. and Chou, Y.-J. (2004). "Tradeoffs associated with sediment-maintenance flushing flows: A simulation approach to exploring non-inferior options." *River Research and Applications*, 20, 591 – 604.

APPENDIX I. EXPERIMENTAL PROCEDURE TO COMPUTE THE EROSION RATE

Image Pre-Processing

Before extracting the laser line position in time, the signal had to be filtered to prevent errors associated with running of water, hiding of laser light behind gravel, fine sediment passing in front of the camera, turbulence wakes, refraction from Plexiglas, and low contrast between laser light and background under gravel crest level. The first filter applied was AMF (Advanced Median Filter), which substitutes the value contained in a cell with the average evaluated on the neighboring cells in a window $2(m \times n)$ in order to reduce noise and intensify signal on laser line (Sung et al. 2009):

$$I_{new}(X,Y) = \frac{\sum_{j=Y-m}^{Y+m} \sum_{i=X-n}^{X+n} I_{raw}(i,j)}{(2n+1)(2m+1)}, \tag{24}$$

where I_{raw} is the unfiltered image, and m and n are the window semi-dimensions, set as 5 and 9 in this work.

The second filter applied was EF (morphological Erosion Filter), which shrinks or thins objects in a gray scale image applying a structural element, in this work a 5×5 square (Gonzalez et al. 2004):

$$I_{new}^{(1)}(x,y) = \min[I_{new}(x+x', y+y') - B(x',y')], \tag{25}$$

for $x' \in (-X, X)$ and $y' \in (-Y, Y)$, where X and Y are the semi-dimensions of the structural element B.

The last filter applied was a THF (morphological Top-Hat Filter) (Gonzalez et al. 2004), which helps remove uneven backgrounds. Applying this filter, a sequence of erosion and dilation is carried out on the original image (in this case the one resulting from the first two filters) via a structural element, once again in this work a 5×5 square. The erosion filter (generating $I_{new}^{(2)}$) is the same described in equation (25), whereas dilation is the opposite procedure:

$$I_{new}^{(3)}(x,y) = \max[I_{new}^{(2)}(x+x', y+y') + B(x',y')]. \tag{26}$$

The final image $I_{new}^{(4)}$ is obtained subtracting $I_{new}^{(3)}$ from the original $I_{new}^{(1)}$. In figure 8, the progressive effect of filtering procedure is shown.

Laser Centerline Extraction

The progressive lowering of the bakelite sediment level over time is mirrored in the decreasing position of laser light over time, as recorded in each video. From each video we extracted a series of consecutive images, each of them represented by a matrix in which each i-row represents the vertical coordinate in pixel and each j-column represents the longitudinal coordinate in pixel, and each cell (i, j) contains the value of the color referred to that pixel. The laser position (corresponding to bed surface) over time was then detected searching the maxima in each column, and counting the number of cells below it. This process leads to a final matrix $T \times X$ in which each x-column (with X elements) still represents the longitudinal coordinate, whereas each t-row (with T elements) represents the time step. The value contained in the (x, t) position therefore identifies the height of the bed in the position x at the time t. The conversion from pixel to mm was given by calibration images. The origin of the vertical axis was set on the gravel crest, identified with Z_{99} of the CPDG.

The height of bakelite sediment over time was then identified by the equation

$$z(x,t) = [Y(x,t) - Y_r]\ H_v\,, \tag{27}$$

where $Y(x, t)$ is the level of bakelite expressed in pixel in position x at time t, Y_r is reference point elevation (= the crest level), and H_v is the vertical scale of conversion from pixel to mm (figure 9). When the bakelite level z is known along the laser line at a certain instant t, the erosion rate in the time step Δt can be easily obtained:

$$E(x,t) = -(1-p) \cdot \frac{z(x, t+\Delta t) - z(x,t)}{\Delta t}\,. \tag{28}$$

Progressive evolution of laser light was extracted for steps of 6, 60, 120, 180, 240, 300 frames. The final analysis was based on 60-frame extraction, corresponding to 2.4 seconds, a time-step below which the erosion rate presents too many oscillating values.

From the information on height and erosion rate relative to a specific point, the analysis was transferred on spatially averaged quantities, excluding non-erodible points (i.e., cells containing gravel):

$$\langle A \rangle (t) = \frac{\sum_{x=1}^{n} A(x,t) \cdot \delta(x,t)}{\sum_{x=1}^{n} \delta(x,t)} \tag{29}$$

where $\delta(x,t) = 1$ if the cell is erodible or $= 0$ if it is not, A is either z or E and n is the number of cells. Non-erodible cells were detected going through each column from the bottom to the top and setting $\delta = 0$ as long as the value contained in the (x,t) cell was the same as the one contained in the $(x, t + \Delta t)$ cell.

List of Tables

Run	I	II	III	IV	V	VI	VII	VIII	IX
d_s [μm]	425	425	500	425	500	425	425	425	425
H [m]	0.030	0.030	0.030	0.050	0.050	0.060	0.070	0.080	0.040
S_0 [-]	0.0024	0.0034	0.0034	0.0014	0.0024	0.0014	0.0014	0.0014	0.0024
B/H [-]	13.33	13.33	13.33	8.00	8.00	6.67	5.71	5.00	10.00
Q [L/s]	3.667	4.267	4.267	5.608	7.033	7.275	8.942	10.617	5.333
u_{*0} [m/s]	0.025	0.029	0.029	0.023	0.031	0.025	0.027	0.028	0.028

TABLE 1. Flow characteristics for the 9 runs. H is the water height from the crest level (Z_{99}), S_0 is the flume slope, B/H is the ratio between the flume width and water height and u_{*0} is the shear velocity at gravel crest level.

List of Figures

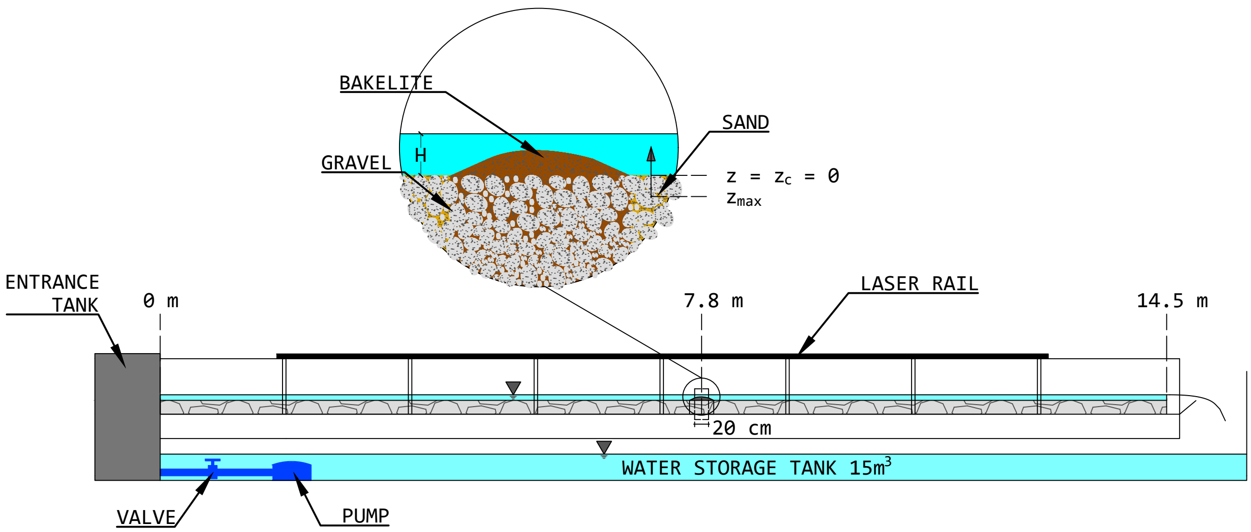

Fig. 1. Flume setup, and (inset) scheme of the initial conditions for the region filled with bakelite.

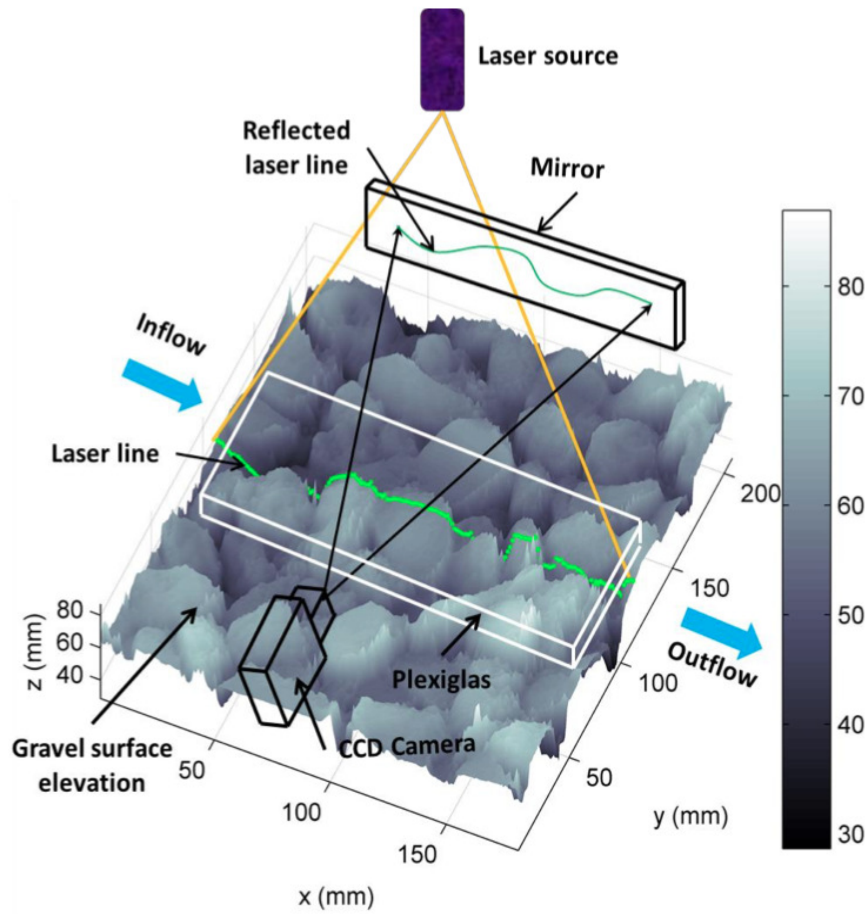

Fig. 2. Laser setup, with the laser line projected on the gravel; the colorbar represents the elevation (mm) (Tarekegn 2015).

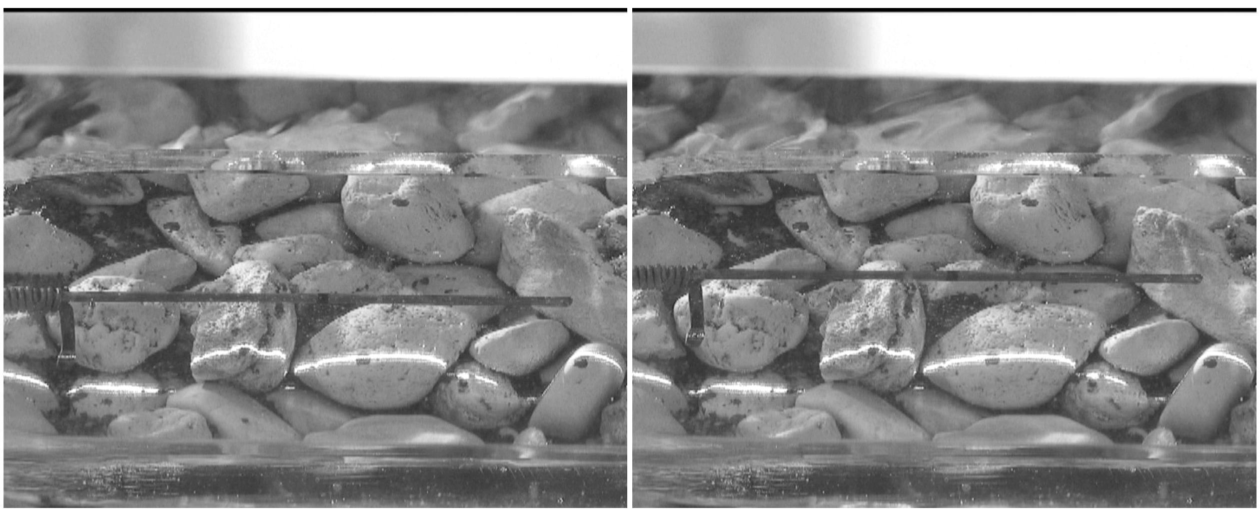

Fig. 3. The calibration rod (104 mm long) moved from position 1 (left) to position 2 (right) by a $\Delta y = 10$ mm.

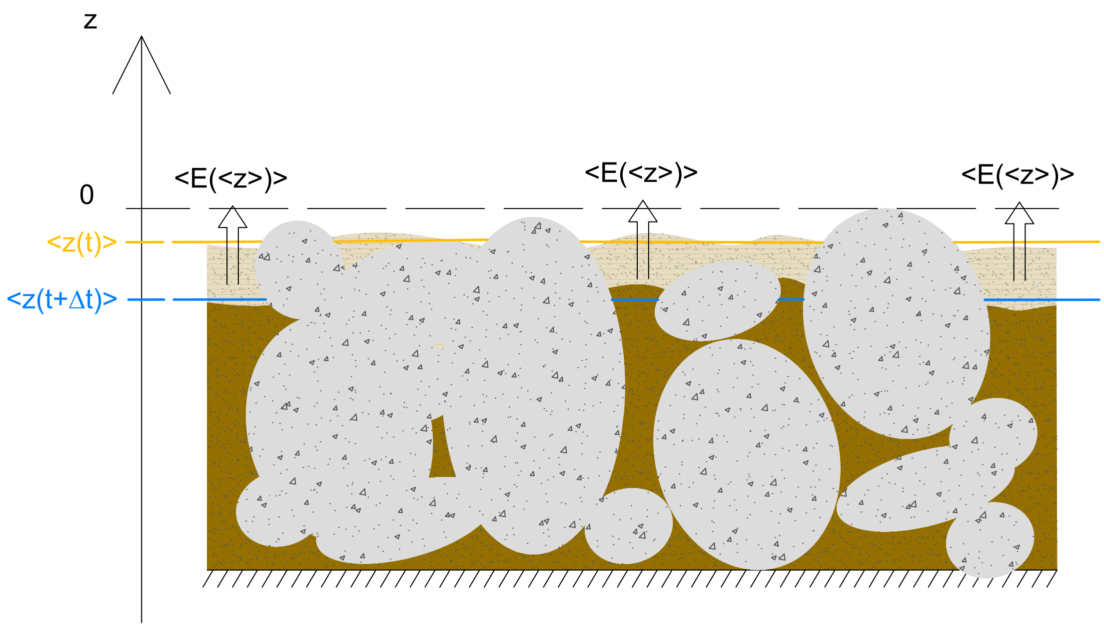

Fig. 4. The erosion rate was calculated by estimating the bakelite-water interface mean elevation $\langle z \rangle$ at different instants t and t $+\Delta$t and applying a finite difference procedure: $\langle E \rangle = -(1-p)\dfrac{\Delta \langle z \rangle}{\Delta t}$ (see Appendix I).

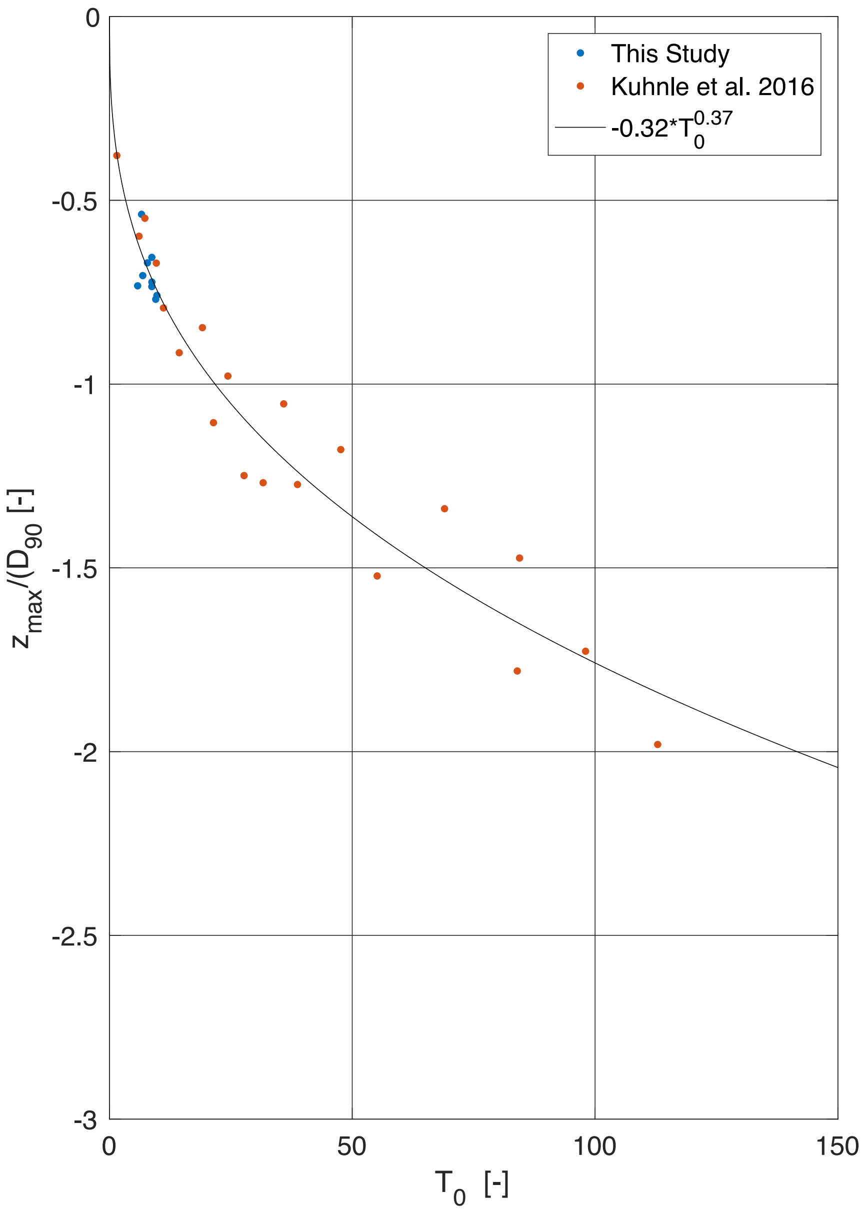

Fig. 5. Measured values of the dimensionless depth of erosion as a function of the dimensionless excess stress, and interpolation using equation (16).

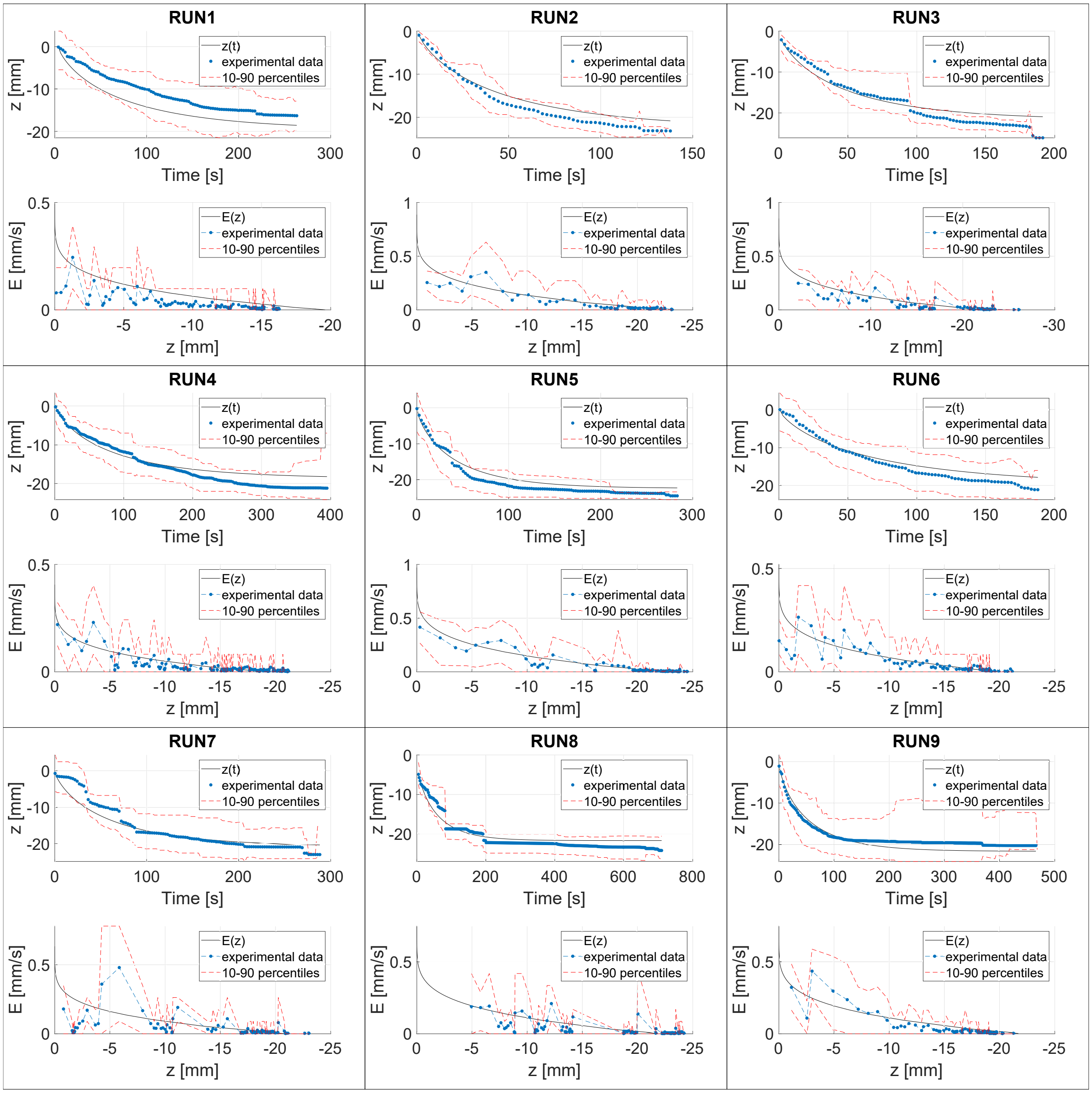

Fig. 6. Temporal evolution of the spatially averaged $z(t)$ and $E(z)$ below the gravel crest, presented with the 10 (lower) and 90 (upper) percentiles from the experimental data distribution at each time t (for $z(t)$) or level z (for $E(z)$). The black solid lines represent the proposed fitting curves (equations 18 and 19).

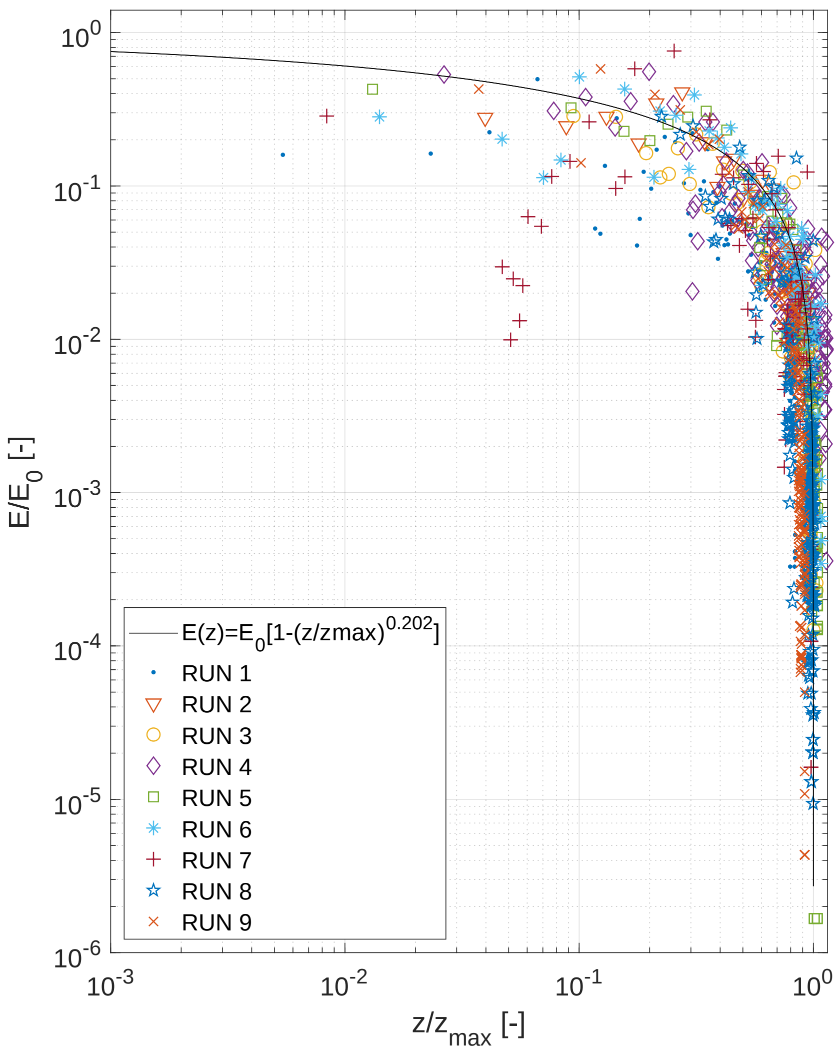

Fig. 7. Measured values of the erosion rate $E(z)$ as a function of the fine sediment level, and the proposed equation (18).

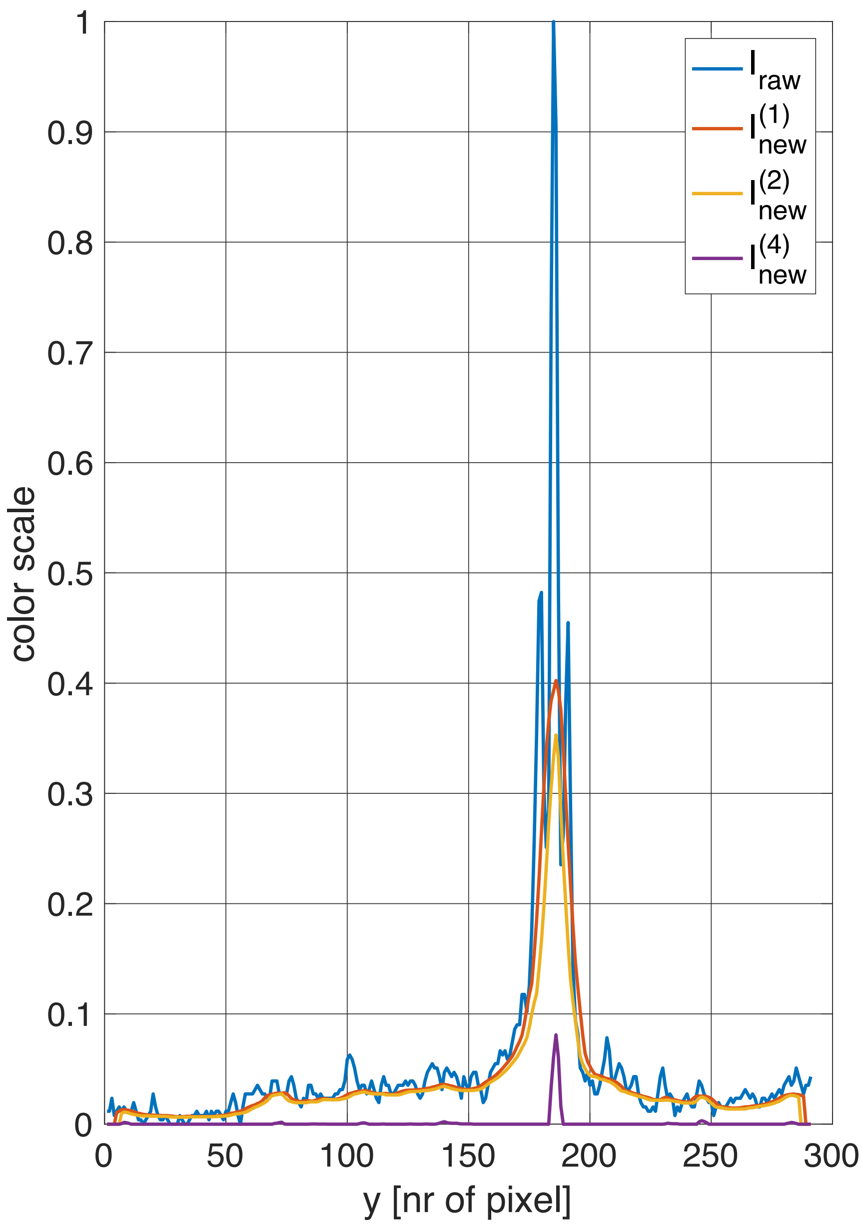

Fig. 8. Progressive filtering of light intensity on the column containing the gravel crest for a frame of the video of Run I.

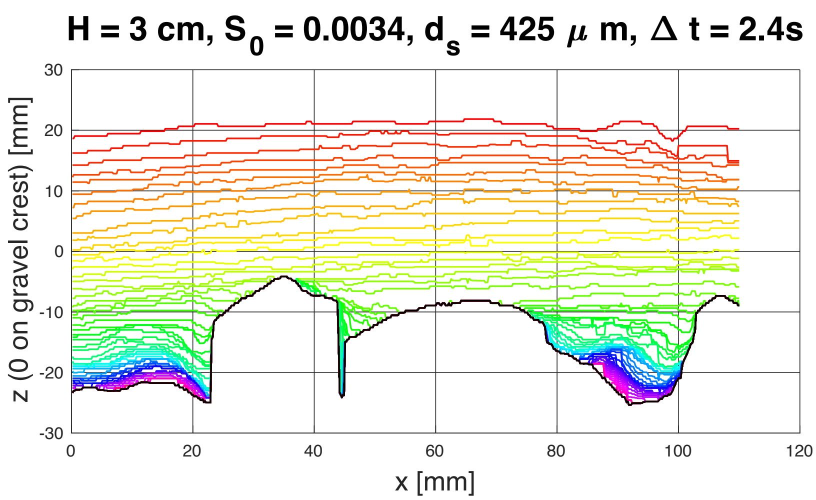

Fig. 9. Evolution of bakelite level during Run II.